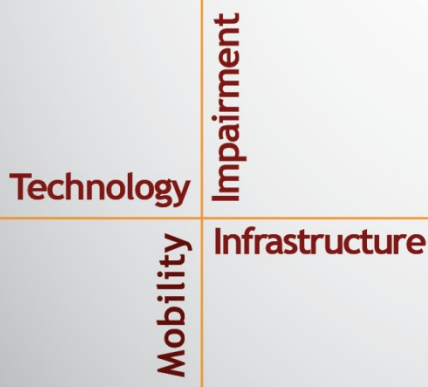# NSTSCE

National Surface Transportation Safety Center for Excellence

Weather Camera

Matthew Palmer • Ronald Gibbons, Ph.D.

Submitted: November 18, 2019

Impairment

Technology

Infrastructure

Mobility

ACKNOWLEDGMENTS

ABSTRACT

Fog- and weather-related visibility reduction is a common cause of multiple-vehicle crashes. Large differential speeds and a tendency of vehicle operators to drive faster than is safe can lead to terrible crashes. Fog can usually be seen on traffic cameras, which are becoming more prevalent on Virginia highways as well as on highways in other states. This project studied the applicability of one approach to using machine vision to measure fog in a realistic environment simulated on the Virginia Smart Road. With the assistance of Dr. Eric Dumont, a leading visibility research from IFSTTAR in France, a machine vision algorithm was applied to video stills captured from a common traffic camera installed on the Smart Road. Machine vision algorithms were used to determine the average loss in visual detail in the scene viewed by the camera and this was used to generate an empirical model relating Meteorological Optical Range (MOR) and the camera images. The model was used to evaluate data captured on days close in time and days over the following year. Finally, the research investigated the approach's sensitivity to preset positioning errors in the camera. The research shows that the approach has promise. However, further research and development are needed before the approach is ready for deployment.

TABLE OF CONTENTS

LIST OF FIGURES

LIST OF TABLES

CHAPTER 1. INTRODUCTION

Adverse weather conditions impair both road safety and mobility. Dense fog, especially, causes multiple-vehicle crashes, some of which are fatal, and often jams traffic for hours. Warning drivers before they enter a foggy road section would help prevent such events by reducing the risk of rear collisions, but requires monitoring meteorological optical range (MOR) locally along the highway. Visibility meters are too costly to be deployed at every location for this purpose. However, closed circuit television (CCTV) cameras are already deployed for monitoring traffic, and offer an opportunity to make MOR measurements at many locations with no additional capital expense.

The Virginia Tech Transportation Institute (VTTI) worked with algorithms developed by the French Institute of Science and Technology for Transport, Development, and Networks (IFSTTAR) and Meteo France (the French national meteorological service) to estimate daytime meteorological visibility with such a camera installed on the Virginia Smart Road. Data were collected under both simulated and real weather conditions.

CHAPTER 2. PURPOSE AND SCOPE

APPROACH

- Install one typical Department of Transportation (DOT) roadside camera (i.e., Cohu Helios Family 3960HD) on the Smart Road near the fog-making systems.

- Adapt software to process the resulting video stream based on research previously performed by IFSTTAR.

- Capture natural or simulated adverse weather conditions to determine the reliability and accuracy of the camera/software system at quantifying adverse conditions.

- Use the existing fog measurement system on the Smart Road to calibrate and quantify the results.

RESULTS SUPPORTING DOT STRATEGIC GOALS

The research will enable DOTs to utilize the newer traffic cameras to detect and quantify fog without permanently installing additional weather stations. This will allow better 511 information for drivers and may enable more advanced speed control that will likely save lives.

CHAPTER 3. METHODS

BACKGROUND

Visibility

Visibility is impacted by the scattering of light by air molecules and any particle in the air. Rayleigh scattering of sunlight by air molecules is responsible for the blue color of the sky, where the blue light is scattered because the wavelength of blue light is approximately the same size as air molecules. Yellow-red light is not scattered as much because these wavelengths are longer and therefore larger than the molecules. The white appearance of clouds and fog is caused by Mie scattering, and is due to the sizes of particles in the air (i.e., the droplets of water in a cloud or fog) being 10–400 times bigger than the wavelengths of visible and near infrared light.

The International Commission on Illumination (CIE) recommends that visibility be defined using meteorological optical range (MOR), which is the distance at which a black object has only a 5% contrast against the sky. Utilizing contrast and the extinction coefficient, an equation can be defined (Equation 1) that allows the calculation of MOR based on extinction ratio k, which has units of 1/unit length (i.e., 1/meters). The extinction coefficient (k) can be measured directly as the loss of light intensity of a beam over a distance.

$$MOR = \frac{1}{k}\ln(0.05) \cong \frac{3}{k}$$ **Equation 1**

Transmissometers operate in this manner by measuring how much light in a collimated beam is lost across a known distance. Airports rely almost entirely on transmissometers to determine visibility. However, transmissometers are expensive and are another inventory item that DOTs would need to maintain in addition to traffic cameras and other safety infrastructure.

Another way to measure visibility would be to directly measure the contrast of an object at a known distance in clear air, and compare that to the contrast measured during a weather event when visibility is reduced. Contrast is defined as the difference between the luminance of an object and the luminance of the background, divided by the overall luminance of the scene. If the object is small and the background is large, the background luminance can be used in place of the total luminance (Equation 2); this is called Weber contrast.

$$C = \frac{I - I_b}{I_b}$$ **Equation 2**

The contrast of the object, C, is a function of the contrast under ideal conditions C_0, k, and distance d, as shown in Equation 3.[1] This formula can easily be redefined as the ratio of the current contrast to the original contrast (Equation 4).

$$C = C_0 e^{-kd}$$ **Equation 3**

$$\frac{C}{C_0} = e^{-kd}$$ **Equation 4**

Further, if C_0 is not known, an equation can be defined for the contrast ratio of two known extinction ratios as C_0 drops out (Equation 5), which then simplifies to Equation 6.

$$\frac{C_2}{C_1} = \frac{e^{-k_2 d}}{e^{-k_1 d}} \qquad \textbf{Equation 5}$$

$$\frac{C_2}{C_1} = e^{-(k_2 - k_1)d} \qquad \textbf{Equation 6}$$

Combining Equation 3 and Equation 6, an equation for MOR with respect to contrast ratio change and distance, d, can be developed (Equation 9). This equation is the basis for many commercial transmissometers:

$$MOR \cong -\frac{3}{\ln\left(\frac{C_2}{C_1}\right)} d \qquad \textbf{Equation 7}$$

One of the challenges of transmissometry is that the equation for MOR (Equation 7) has the natural logarithm of the contrast ratio in the denominator. As the extinction ratio approaches zero, the contrast ratio of C_2/C_1 approaches one and the equation approaches infinity because the natural log of one equals zero. The equation is thus considered ill-posed due to the denominator approaching zero. The equation becomes very sensitive to error in the measurement of the contrast ratio at medium to large MOR, and small errors in the measurement of contrast can result in very large MOR errors. Many transmissometers artificially limit the maximum MOR output to minimize the effect of error in the contrast measurement at higher MOR.

One common method of reducing the impact of error on an ill-posed equation is to use a smoothing function to reduce the error in the measurements before calculating the desired measurement. The most common smoothing function is a boxcar average over time, but this may result in considerable delay in the measurement of transients and considerable underestimation of fog density. An alternative would be to average multiple measurements simultaneously, which is another advantage of using a camera to make the contrast measurement. With a traffic camera, potentially millions of contrast measurements could be averaged together to reduce the noise of a single MOR measurement. If the noise in the measurement is Gaussian, 1 million pixels could reduce the noise in the measurement of contrast by 30 dB (1,000 times), which would help mitigate the ill-posed nature of the calculation.

IFSTTAR Method and Software

IFSTTAR and Meteo France developed algorithms and a software toolbox to process digital camera images for measuring MOR. The approach is based on measuring the amount of detail in an image and comparing that detail amount to the amount of detail present when there is no fog. VTTI used these algorithms to develop software utilizing the hardware installed at VTTI and typically used by the Virginia Department of Transportation (VDOT). The software developed by VTTI was optimized for research.

The detail in an image is related to the contrast of the many objects in the scene and many camera-specific factors. However, if two images are taken by the same camera at a fixed focus point and all other factors remain unchanged, the difference in detail between the two images can only be affected by changes in the contrast of the objects in the scene.

Detail in an image can be measured as a summation of all of the pixels of contrasting objects in an image. Since detail represents the contrast of many objects in a scene at many distances from the camera, it should be more robust than measurement of contrast of a single object in the presence of real-world noise such as traffic, animals, etc., as each of these only affect a small number of pixels at a time.

The IFSTTAR/Meteo France approach[1] measures the details in a digital image by processing the image with a Sobel gradient edge detection algorithm. Edge detection, like the Sobel gradient, enhances the contrast of an object in an image by approximating the first derivative of the changes in pixel intensity. It emphasizes areas where the color or intensity changes rapidly and de-emphasizes slow changes. This is useful for finding discrete objects in machine vision by locating their edges.

The Sobel gradient uses integer matrix math to approximate the first derivative and is thus computationally inexpensive. The Sobel gradient processes the image by convoluting two operators, G_x and G_y, with each pixel and its eight immediately surrounding pixels. G_x enhances the horizontal edges or gradients and G_y enhances the vertical edges. Equation 8 shows the masks G_x and G_y.

$$G_x = \begin{bmatrix} +1 & 0 & -1 \\ +2 & 0 & -2 \\ +1 & 0 & -1 \end{bmatrix} * I \quad \text{and} \quad G_y = \begin{bmatrix} +1 & +2 & -1 \\ 0 & 0 & 0 \\ +1 & -2 & -1 \end{bmatrix} * I \qquad \textbf{Equation 8}$$

G_x and G_y are then vector summed for each pixel as shown in Equation 9.

$$G = \sqrt{G_x^2 * G_y^2} \qquad \textbf{Equation 9}$$

The color images are converted to grayscale in order to convert the pixels into a measure of the relative contrast of the scene. The Sobel gradient then enhances the contrast changes to improve the measure of changes in the contrast. The gradient, G, from the Sobel process for each pixel is then summed to represent the overall detail of the image.

Shadows and specular reflections can add noise with this approach because they create contrast changes that are not related to the extinction ratio. Specular reflections are high luminance reflections from a smooth or polished surface, such as a car windshield or a mirror. Other objects that pass in and out of view, such as vehicles on the roadway, can also add noise to the measurement of detail.

To minimize these noise sources, the IFSTTAR/Meteo algorithm[1] also weights each pixel via a Lambertian map that represents the Lambertian surfaces in the scene. A Lambertian surface is a surface that has a diffuse or rough surface that reflects all illumination evenly in all directions.

These objects have a brightness that more or less correlates with the sky brightness. The Lambertian map is an image generated by calculating a correlation between each pixel and the relative brightness of an area of the image showing the sky. This method works despite the use of automatic gain and automatic shutter speed by the traffic cameras since the ratio between the sky pixel intensity and the diffuse object pixel intensity will not change with variations in gain or shutter speed as long as the view of the sky does not include a direct image of the sun.

A high correlation coefficient—r, near +1 or −1—would mean that a particular pixel is measuring a Lambertian surface. The pixels from Lambertian surfaces correlate well with the intensity of pixels from the sky throughout the daylight hours. The algorithm uses the determination coefficient, R^2, to weight each pixel's contribution to the summation of the scene's details in the image. This reduces the impact of specular reflections and shadows on the calculation of contrast change.

EXPERIMENTAL DESIGN

The experimental design for this project used uncontrolled variation in weather and the presence of very light traffic. A traffic camera was installed on the Smart Road a short distance from the paved lanes. Video data were collected over two periods to collect both natural and simulated fog events. The video was processed with machine vision algorithms to relate MOR to the level of detail visible in the video scene. A model was developed with the data from one day and tested utilizing different days and events to simulate a real-world implementation.

Data Collection Time Period

Data were collected during the month of September 2015 and from late April to December 2016. During these times, data were simultaneously collected from both the visibility meter and the camera. Table 1 shows the dates that weather events were captured during September 2015, the timing of the events, the type of weather, and whether it was natural or man-made (simulated). Any event that contained mixed weather conditions could not be used to develop the model. Additionally, fog needed to be simultaneously visible in the video scene and measurable at a weather station located near the camera. Due to these factors, only the events on September 17, September 23, and September 24 were suitable for the experiment.

In an extension to the project, data collection continued from May to December in 2016. During this period, an attempt was made to capture two fog events surrounding an intentional movement of the camera away from and back to the established preset in order to test the sensitivity to positional error. These data were also used in the characterization of the camera's performance. The list of weather events is included in Appendix A.

Table 1. Data collection period and details.

Event Date	Event Start	Event End	Event Type	Duration, hr:min	Intensity	Natural/Simulated
10-Sep-15	11:09	11:42	Rain	0:33	Very Light	Natural
10-Sep-15	13:56	14:29	Rain	0:33	Very Light	Natural
10-Sep-15	15:02	16:26	Rain	1:24	Very Light	Natural
11-Sep-15	6:24	9:21	Fog	2:57	Light	Natural
13-Sep-15	8:38	9:45	Fog and Rain	1:07	Light	Natural
16-Sep-15	7:14	8:21	Fog	1:07	Light	Natural
17-Sep-15	6:40	10:01	Fog	3:21	Light	Natural
18-Sep-15	6:41	8:55	Fog	2:14	Light	Natural
19-Sep-15	6:41	8:01	Fog	1:20	Very Light	Natural
20-Sep-15	7:32	8:39	Fog	1:07	Very Light	Natural
21-Sep-15	6:57	11:48	Fog and Rain	4:51	Light	Natural
21-Sep-15	17:55	19:02	Rain	1:07	Very Light	Natural
22-Sep-15	8:22	9:45	Fog	1:23	Light	Natural
23-Sep-15	8:04	8:54	Fog	0:50	Light	Simulated
23-Sep-15	9:44	10:01	Fog	0:17	Light	Simulated
24-Sep-15	6:42	9:29	Fog	2:47	Light	Natural/Simulated
25-Sep-15	6:57	7:14	Rain	0:17	Very Light	Natural
25-Sep-15	8:21	15:18	Rain	6:57	Light	Natural
25-Sep-15	15:52	16:08	Rain	0:16	Very Light	Natural
26-Sep-15	6:58	12:49	Fog and Rain	5:51	Very Light	Natural
26-Sep-15	14:12	20:03	Rain	5:51	Very Light	Natural
27-Sep-15	7:31	19:45	Fog and Rain	12:14	Very Light	Natural
28-Sep-15	6:58	11:09	Fog	4:11	Light	Natural
28-Sep-15	13:06	13:39	Rain	0:33	Very Light	Natural
28-Sep-15	18:06	19:46	Rain	1:40	Very Light	Natural
29-Sep-15	17:15	19:45	Fog	2:30	Light	Natural
29-Sep-15	7:14	15:01	Fog and Rain	7:47	Medium	Natural

Camera

The camera selected for the study was a Cohu Helios Family 3960HD. The camera was recommended by VDOT personnel and purchased by VTTI. The camera was installed on the Smart Road on a 150-millimeter (6-inch) diameter pole 6.1 meters tall, 7 meters to the southwest of the Vaisala weather station and 15.2 meters from the center of the Smart Road's two paved lanes. The camera view was turned southeast to view that portion of the Smart Road. The camera specifications and settings are shown in Table 2.

Table 2. Cohu camera specifications and settings.

Specification	Setting
Defog	off
Image Stabilization	off
Resolution	1280×720 pixels
Frame Rate	1 frame / second
Recording Format	H.264
Shutter/Integration	auto
Iris	auto
Focus	auto
Zoom	fixed at minimum
Repeatability of Preset Position	± 0.25 degrees
S/N Ratio	> 50 dB

Weather Station and Fog Measurement

A VDOT Vaisala weather station installed 8.2 meters from the center of the paved lanes of the Smart Road was utilized to measure fog at the camera location. A Vaisala PWD22 sensor was utilized to capture visibility data. The sensor specifications are shown in Table 3.

Table 3. Vaisala visibility sensor specifications.

Specification	
Range	10–2000 m
Accuracy	±10%
Operating Principle	Forward Scatter
Sample Rate	1 per 5 minutes

Figure 1 illustrates the relative positions of the weather camera, the weather station, and the Smart Road lanes. Also shown is the approximate view of the camera. The camera view was oriented to encompass as much of the Smart Road as possible from the location near the weather station.
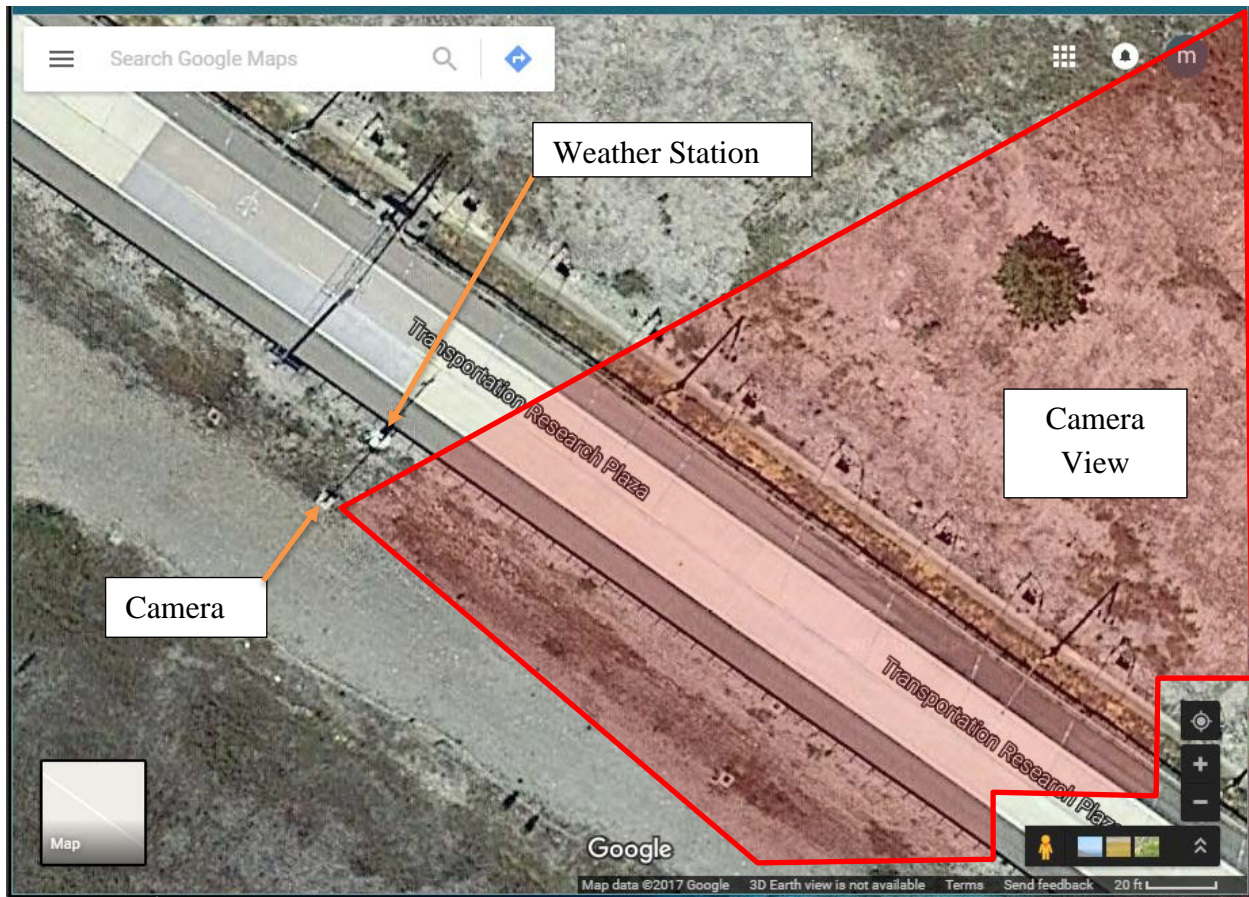
Figure 1. Map. Relative position of weather camera, weather station, and Smart Road.

DATA ANALYSIS

The video data were reduced by extracting stills from the video captured from the Cohu camera utilizing custom software intended to interface with that camera. The stills were extracted approximately every 5 minutes to match the sample rate of the Vaisala PWD22 sensor to prevent interpolation error. The stills were then processed with custom machine vision software utilizing the IFSTTAR/Meteo algorithm. A model was developed and fitted to a single-day event and then used to calculate the MOR from the stills. The calculated MOR was then compared to the MOR measured by the weather station. Camera-measured MOR errors were calculated and analyzed with respect to the observed fog in the stills. Analysis of variance (ANOVA) was used to analyze the errors with respect to type of event (simulated or natural), MOR, and season. Qualitative analysis (i.e., observation of image features captured from the stills) was also utilized to determine potential causes of error in the camera-measured MOR.

CHAPTER 4. RESULTS

SUMMARY OF FOGGY DAYS

The project initially focused on two simulated fog events in the initial data collection of 2015. These were the two simulated fog days on September 23 and 24, 2015, which generated a large range of MORs. No other days collected in 2015 were suitable for calibration of the camera due to lack of sufficient fog samples.

Figure 2 shows the average detail calculated from the camera video stills and measured MOR data from September 24, 2015, for a simulated fog event. Figure 3 shows a similar event from the previous day with the night data removed. Since the Smart Road is unlit, the average detail visible during the night (15,000–40000 and 88,000–100,000 seconds) is much lower than the average detail visible during the day (42,000–85,000 seconds). This confirms that there is a need for the roadway to be lighted if the system is intended to function at night. Another feature of the average detail is that the detail changes throughout the day by a fairly large percentage: by 10%–15% of the full range. However, since the PWD22 sensor has an upper limit of 2,000 meters for MOR, it could be possible that the actual MOR varied this much during the day. As expected, the average detail drops during the simulated fog event. This is also indicated by the measured MOR, which also dropped during the same approximately 1.9-hour time period. Figure 3 and Figure 2 show similar results.
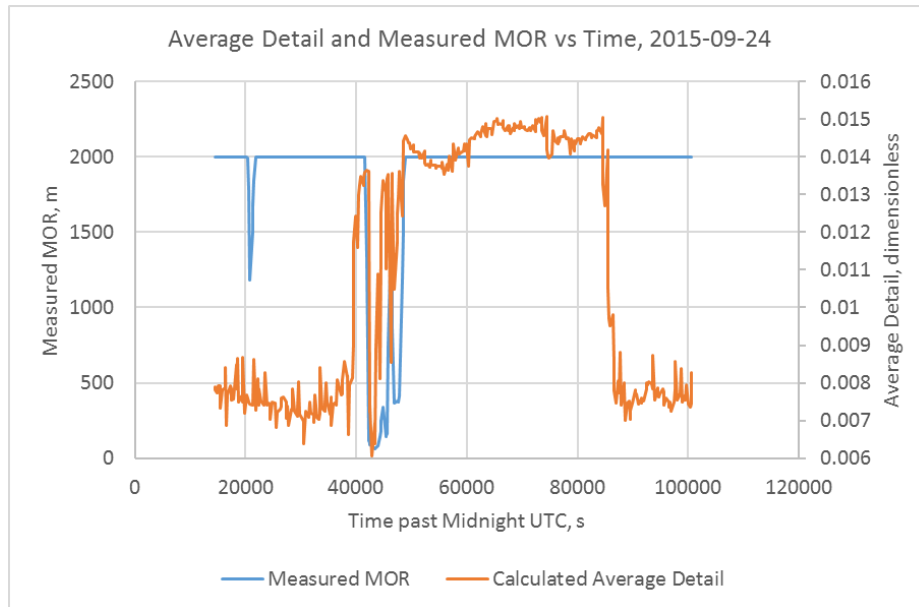
Figure 2. Graph. Calculated average detail per video still and measured MOR vs. seconds past midnight UTC, September 24, 2015.
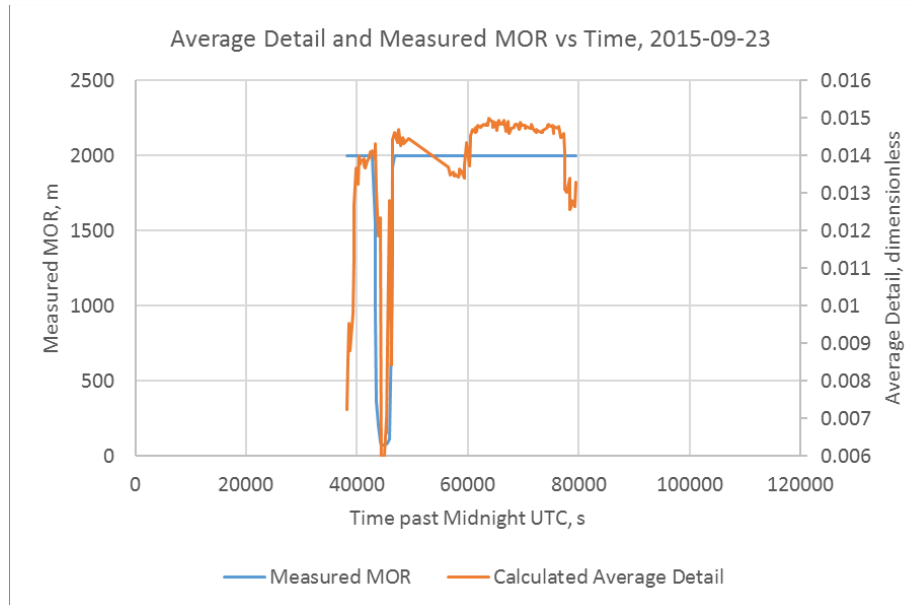
Figure 3. Graph. Calculated average detail per video still and measured MOR vs. seconds past midnight UTC, September 23, 2015, only the daylight hours.

DAYLIGHT CALIBRATION AND LAMBERTIAN MAP

In order to generate a Lambertian map, a sunny day with few or no clouds was needed. The data collected on September 15, 2015, were used (Figure 4). The cloudless blue sky needed for the correlation calculation can be seen in the background. In addition to the requirement for blue sky, these data were selected due to season (late summer) and proximity to the simulated fog events. The thinking was that the late-summer Lambertian map would have the most vegetation and thus the most specular reflections of any of the seasonal video captures and would result in the most conservative Lambertian map, and therefore would be applicable to the rest of the year.

14

Figure 4. Photo. Smart Road weather camera image, September 15, 2015, 2:10 p.m.

Using the video stills from the daylight hours of September 15, 2015, a Lambertian map was generated (shown in Figure 5). The pixels are grayscale, where white equals a weighting factor of one while black equals a weighting function of zero. The Lambertian map reduces the roadway's influence on the calculation of average detail, which is expected given the specular nature of roadway surfaces. The map also removes most of the visible vegetation from the calculation in the near field, but keeps the mountain in the background. The sky area is the largest area of high influence (white color), but probably results in little added detail in the calculation even in the presence of partial cloud cover.

There is some smearing of the pixels, which is especially evident in the tops of the mountains in the background. The smearing was likely due to thermal expansion and deflection due to wind. The high and low temperatures on that day were 81 °F and 49 °F. The wind also varied between 0 and 8 miles per hour with a maximum of 12 miles per hour recorded. This represents a real-world challenge that traffic camera-based weather stations will need to handle.

Figure 5. Image. Lambertian map of the Smart Road traffic camera installation, September 15, 2015.

The video stills used to calculate the Lambertian map were then processed with the MOR algorithm. The results (Figure 6) show that the average detail varies approximately 20% throughout the day, but in general is relatively flat. The average detail is very low at night due to the lack of roadway lighting before 35,000 seconds and after 85,000 seconds. These data are similar to the average detail from the fog event shown in Figure 2. The periodic increase in noise at night is due to the camera picking up glare from its own flashing LED power indicator. The periodic noise data were compared in post hoc analysis to the video, which showed the LED flashing. Finally, dusk and dawn are nonlinear due to the camera compensating for the light level changes and due to shadowing of the Smart Road scene.
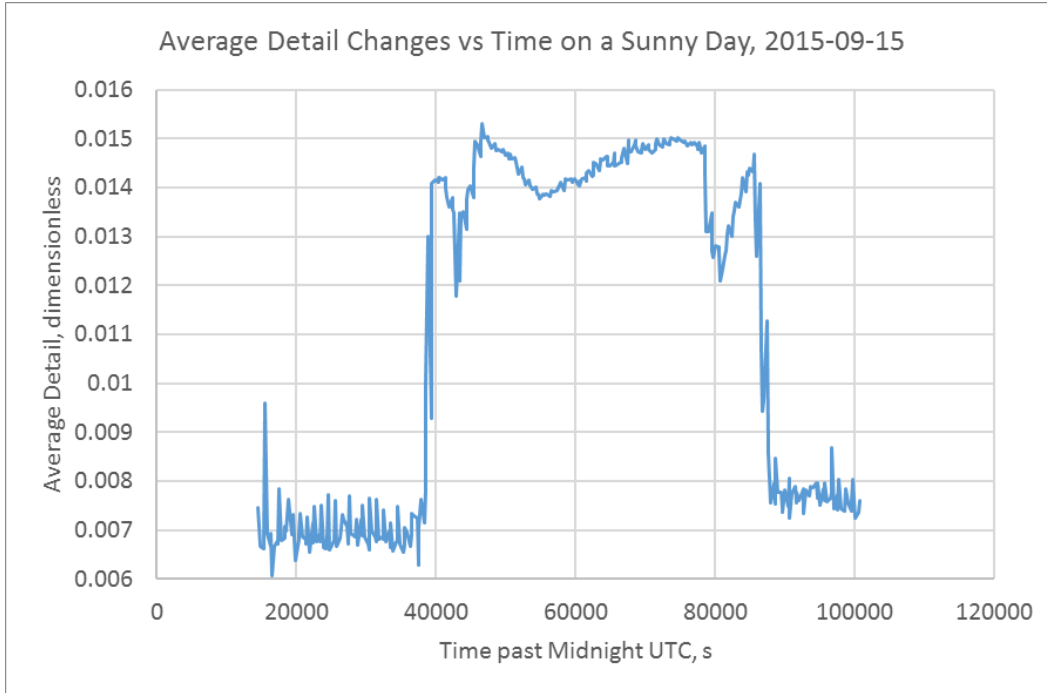
Figure 6. Chart. Average detail calculated from video stills, September 15, 2015.

CALIBRATION USING SIMULATED FOG

Figure 7 shows the data calculated from the video stills during a simulated fog event on the morning of September 24, 2015. The graph shows the average detail, a dimensionless quantity, versus the independently measured MOR. The graph also shows a model of the interaction between MOR and average detail.

The model is based on Equation 9, which relates MOR, distance, and contrast ratio. The generic form of the model used is shown in Equation 10, where a is a multiplier relating average detail and contrast ratio, d is average distance from the camera, and c is an offset coefficient. The average detail of each frame is substituted for C_2 and the average detail of the Lambertian map is substituted for C_1.

$$MOR \cong -\frac{3}{\ln\left(a\frac{C_2}{C_1}\right)}d + c$$ **Equation 10**

The coefficients a, c, and d of the model were fitted using a nonlinear least squares methodology. The coefficient for d suggests that the average distance from the camera for all of the pixels in the view is 20.26 meters. The multiplier a implies that the maximum average detail ratio from this scene will be less than 0.0149, which would result in the denominator being zero. The offset c was utilized in case there was a systematic error in the MOR measurement. The determination coefficient (R^2) for the fit was 0.62 (i.e., 62% of the variance was explained by the model).

17
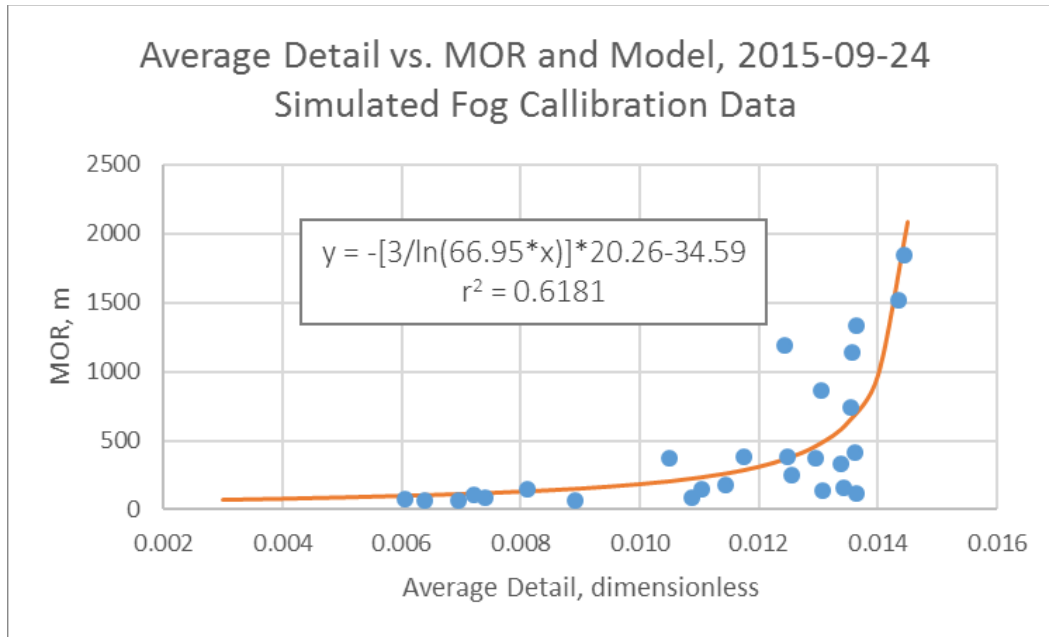
Figure 7. Chart. Average detail vs. measured MOR calculated from video stills during a simulated fog event, September 24, 2015.

The data points used for the calibration only included data with a MOR less than 2,000 meters. Since the weather station's upper limit for MOR was 2,000 meters, any measurement of exactly 2,000 meters could be any MOR $\geq$ 2,000 meters, and therefore unknown. No nighttime data were included because the camera view was not lighted.

Finally, an outlier was removed from the data before calculating the model fit. This data point corresponded to 08:52:24 or 46,344 seconds past midnight UTC. For this video still, the average detail calculated was 0.0085 for a measured MOR of 1,495 meters. This particular video had a number of issues (Figure 8) that justified its removal. Since this was a simulated event, the fog was not fully developed and not uniformly distributed. Therefore, the weather station, which is just out of sight at the bottom left of the camera view, was not sampling the fog that the camera was seeing. In addition, the sun was nearly in the camera's view, resulting in lens flares. Further, the top of the vehicle on the road was generating a specular reflection, so the camera adjusted the shutter time to compensate for the increased brightness, resulting in a loss of image detail that is not due to fog. Lens flares and specular reflections are additional challenges that a traffic-camera-based weather station will need to handle in real-world application.
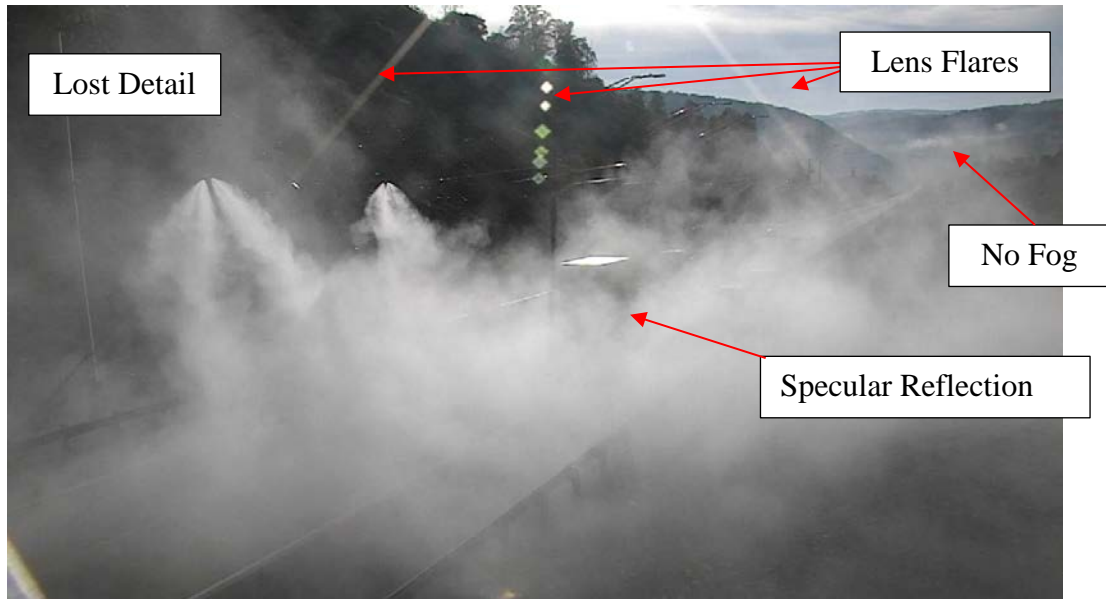
Figure 8. Photo. Video still, September 24, 2015, 08:52:24 a.m.

The calculated MOR using the calibration from September 24, 2015, is shown in Figure 9. The data points in the ellipse show that the camera output was invariant at approximately 690 meters for MORs ranging from 100 to 1,300 meters as measured by the weather station. This lack of change in the camera MOR indicates a lack of correlation with the weather station MOR. This indicates that these data and calibrations were not suitable for the generation of the calibration curve. In addition, the residuals (Figure 10), exhibit a nonuniform distribution that further suggests a problem with the calibration or Lambertian map. These errors in the camera-measured average detail were due to nonuniformity similar to that illustrated in Figure 8. The data analysis continued with a calibration generated from a natural fog event in 2016. However, in order to test the applicability of the Lambertian map approach across all seasons, the Lambertian map was not changed.
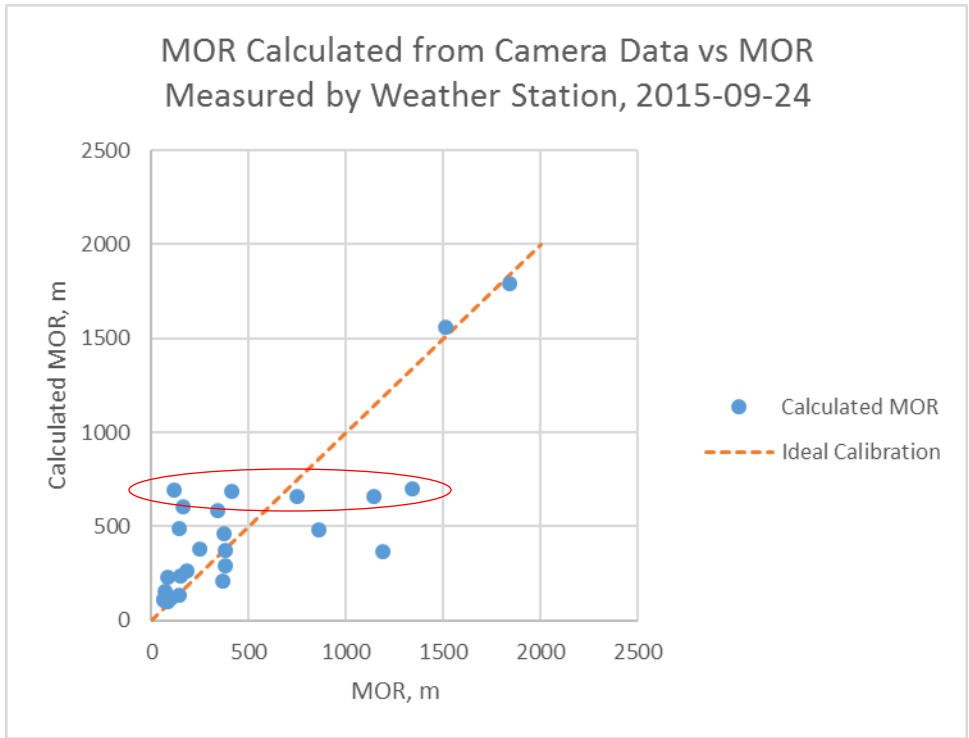
Figure 9. Chart. Calculated MOR from simulated fog calibration on September 24, 2015.
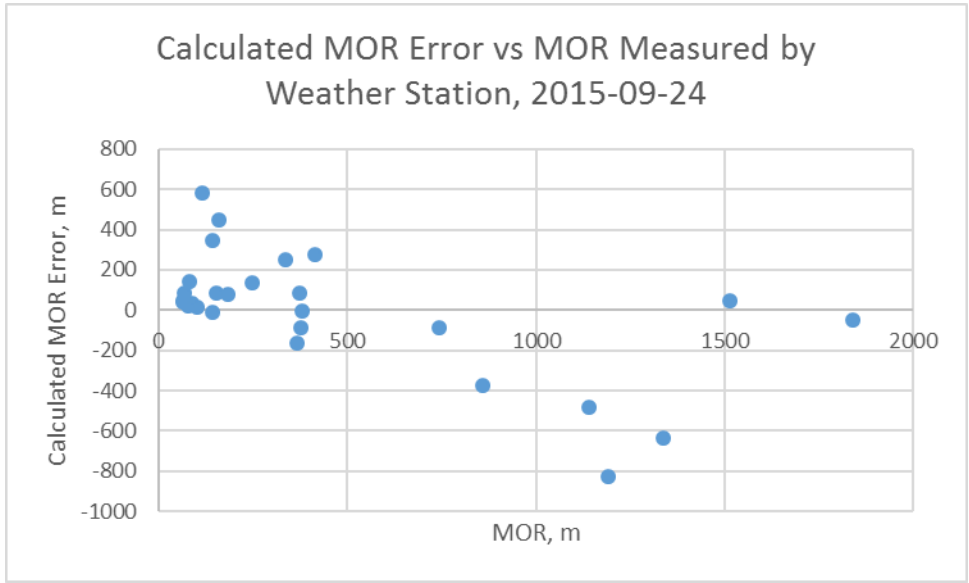
Figure 10. Chart. Calculated MOR residuals (error) in the calibration from September 24, 2015.

CALIBRATION USING NATURAL FOG

A calibration model was also completed using data collected from a natural fog event from late 2016. This calibration appears to be a better fit of the model than the simulated data. This data set had the most variation in MOR of all the captured natural events.

A natural fog event in 2016 was used to create another model of the interaction of the reduction in average detail from camera images and the MOR measured at the weather station. Again, only the data where MOR was less than 2,000 meters were used. The average detail versus the MOR measured at the weather station is shown in Figure 11. The lowest MOR for this event was 266 meters. The calibration model is also shown.

The average detail in the scene, as measured by the camera between 266 and 600 meters MOR, is relatively well correlated with lower variance compared to the data above 600 meters MOR. The calibration coefficients are different from the fit to the simulated fog. In this case, the average distance of the pixels from the camera, d, is 80.6 meters, and the offset c is 0.988. However, there is only a slight difference in multiplier b between the simulated and natural fog events, at 66.95 and 62.32. Finally, the goodness of fit was better for the natural fog event, with $R^2 = 0.67$. This model was used for the remainder of the analysis of performance.
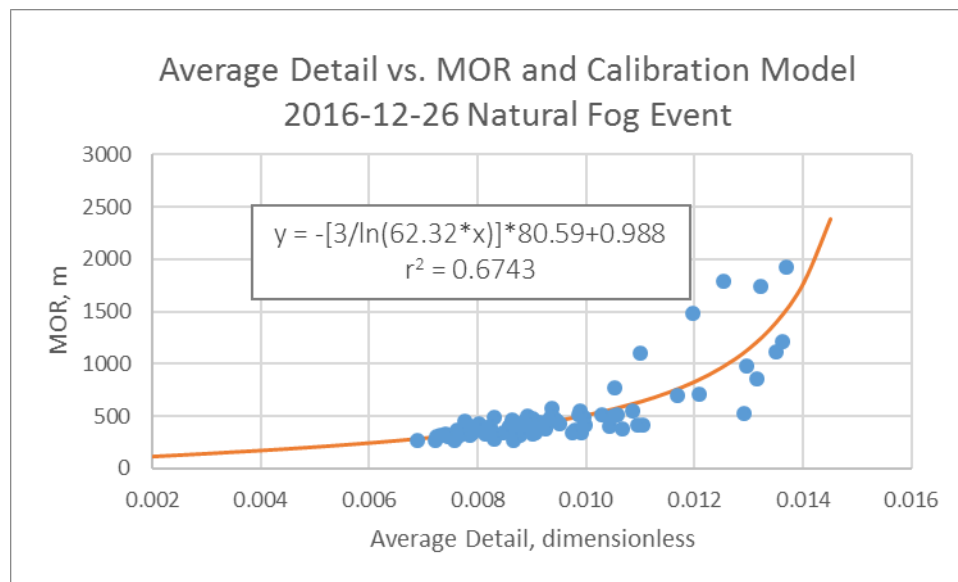
Figure 11. Graph. Average detail vs. MOR and calibration model for natural fog event on December 26, 2016.

TESTING GOODNESS OF FIT ON CALIBRATION DATA

Figure 12 shows the MOR calculated using the calibration data and the ideal calibration relationship for reference. This illustrates the amplification of noise caused by the ill-posed nature of the relationship. The largest error in the calculated MOR, highlighted in red in the chart, is 582 meters more than the 527 meters MOR the weather station reported. This is a 52% error based on the measurement by the camera and is a false negative; i.e., the camera is reporting better visibility than the weather station. Since MOR is a safety-critical measurement, a

large false negative is a serious concern, as it would not be used to issue a warning for drivers to slow down. However, this MOR is much larger than the safe stopping distance of 250 meters at 120 kilometers per hour,[2] and the errors are reduced as lower MORs are approached. Thus, MOR calculated using this calibration data could be used for a reduced visibility sign or warning lights with some averaging of the measurements to reduce scatter.
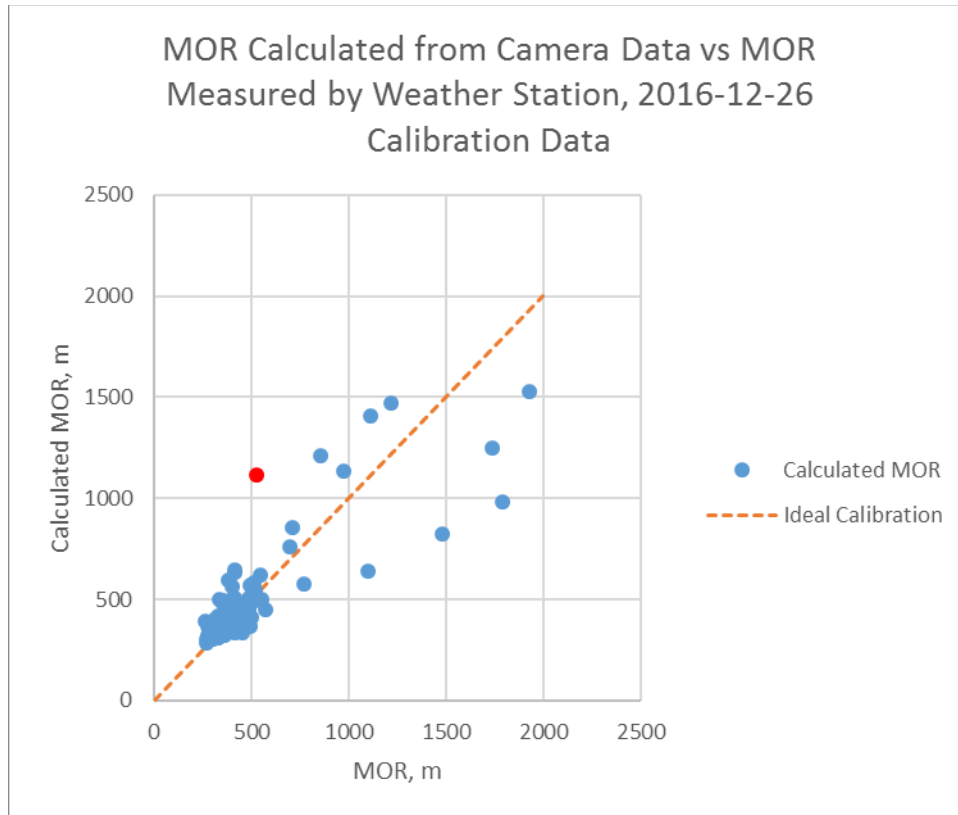
Figure 12. Graph. MOR calculated from the weather camera calibration vs. MOR measured by the weather station, December 26, 2016, calibration data.

TESTING ON NON-CALIBRATION DATA

The calibration from December 26, 2016, was then applied to data captured in 2015 and for all seasons in 2016. Figure 13 shows the MOR calculated from the camera stills for the days listed in the legend. As the figure shows, there is considerable scatter in the MOR error as well behavior changes. Trend lines fitted to the data show that the slope and offset of the error depend on the day and the type of event. The ideal calibration response is also shown as a straight line where each calculated MOR is equal to the actual MOR. In addition to the date collected, the data are marked natural or simulated for the type of event.

Since the calibration curve should linearize the camera measurement, each day's data set should follow a straight line from (0, 0) – (2000, 2000) like the ideal curve. However, this is not the case. The natural event from September 29, 2016, is the only data set that exhibits the correct behavior. All other data sets exhibit either the wrong slope, a large offset, or both. The data from September 23, 2016, have nearly the correct slope, but an offset of approximately 400 meters.

22

Most of the natural data have a negative offset and a slope that is too shallow. This suggests that the calibration and/or Lambertian map does not apply to all seasons.

The data show that the simulated events have the largest error for a small MOR, likely because of the nonuniformity of the simulated fog versus natural fog. The natural events have a slightly lower average MOR error of −340 ±54 meters overall, while the simulated fog events have an average MOR error of 434 ±69 meters based on the ANOVA. These data illustrate the challenges associated with the approach.
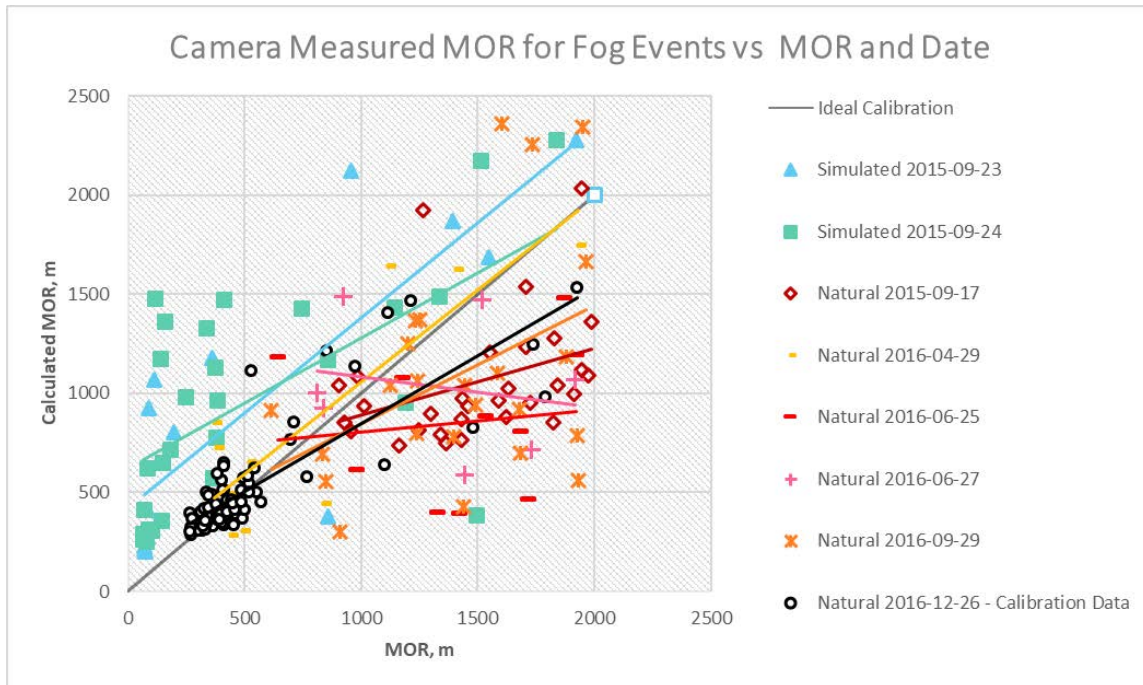
Figure 13. Graph. Calculated MOR vs. measured MOR for various natural and simulated fog events, including the calibration data.

Figure 14 illustrates the fog nonuniformity problem. In these stills, approximately 2.5 minutes apart, the mountains in the background are barely visible in one still due to fog and completely visible in the next. The Lambertian map (Figure 5) includes the mountain in the calculation, which, depending on the correlation weighting, might account for 7%–10 % of the average detail measurement. However, in neither case is there visible fog present in the foreground near the weather station used for calibration.

Figure 14. Photo. Subsequent video stills illustrating the nonuniformity of the fog.

Figure 15 illustrates the average MOR errors versus MOR ranges. Shown are the average errors for ranges of MOR for both simulated and natural event types. To produce this analysis, the errors for each MOR were binned based on the ranges shown on the *x*-axis. The error bars represent the standard error of the averages at each binned MOR. As the figure shows, the simulated event has, in general, more variance in each average than the natural fog events. In addition, the camera MOR measurement error with respect to MOR varies less predictably for the simulated event versus the natural events. Statistical analysis found the differences in interaction to be statistically significant with a $Pr > F$ of 0.015. Based on Figure 15 and **Error! Reference source not found.**, the simulated events were removed from further analysis due to applicability concerns.
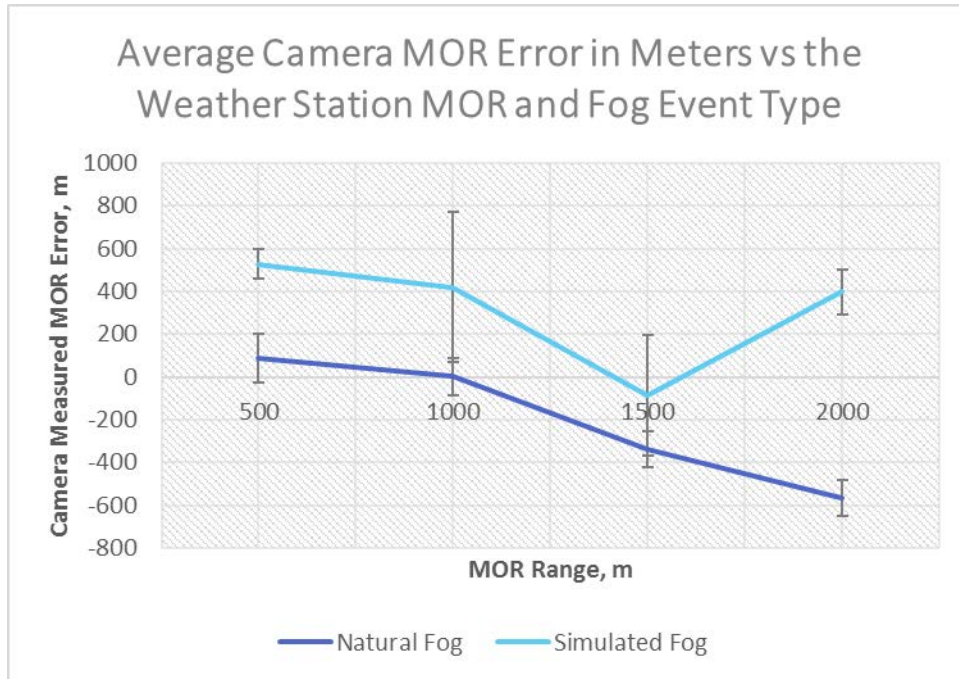
Figure 15. Graph. Average camera-measured MOR error in meters vs. the weather station MOR and event type, not including calibration data.

The data were sorted into a finer, near geometric distribution of MOR ranges. A geometric distribution was chosen since the stopping sight distance is proportional to the square of the velocity. The finer distribution was chosen to see if the chosen ranges were masking the calibration error behavior.

There is a nonsymmetric distribution of the average errors with respect to MOR, as shown in Figure 16. The errors are shown on equal *x*- and *y*-axis scales to illustrate the scaling of the error. A line fitted to the error averages shows that the calibration is not optimized for the whole data set; there is a systematic error or residual left, which usually signifies that the model is not fitting the data well. This could be due to the model formulation, or could be due to other errors, such as calibration or seasonal changes in the scene that are not normalized by the Lambertian map.
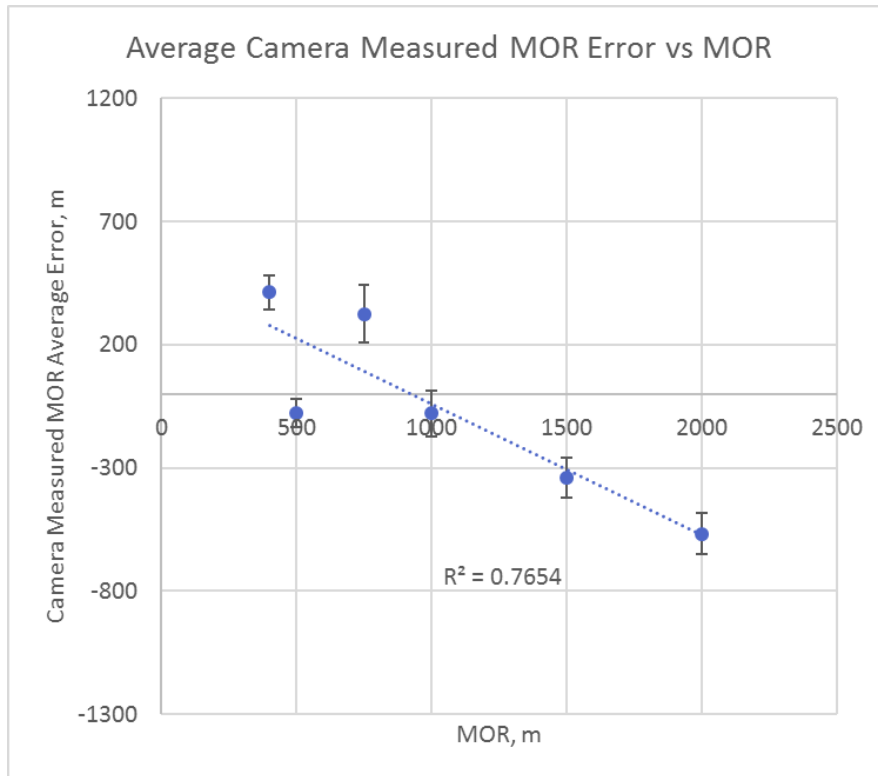
Figure 16. Graph. Average camera measured MOR errors vs. MOR for all natural fog events, excluding the calibration data.

The mean camera-measured MOR errors with respect to dates and seasons are shown in Figure 17. The error bars represent the standard error for these mean MOR errors. The data do not include two full years of samples; however, there are data from late summer and fall over two years with spring and winter each sampled once. Since the calibration utilized the data from December 26, 2016, the average error and scatter are smallest at that point. The mean error from September 17, 2016, is similar to the mean error from June 25 and June 27, 2016, but slightly different from September 29, 2016. All of these dates exhibit mean errors with a large negative offset. There is a big difference in the mean errors between June 25 and June 27, 2016, but this could be due to the large variance in the data. The simulated data are considerably different from the rest of the data captured with a large positive offset. The mean errors from April 29, 2016, were the least different from the calibration data, with a 76 ±90-meter offset.

Excluding the simulated data events, there is a cyclical pattern to the errors in the calculated MOR. This suggests there is a seasonal variance in the detail that cannot be accounted for by the Lambertian map in this approach, despite the flattening of the detail changes throughout a single day. One solution to this challenge may be to capture seasonal calibration images, convert those to additional Lambertian maps, and write algorithms to linearly interpolate between those maps using the date and time.
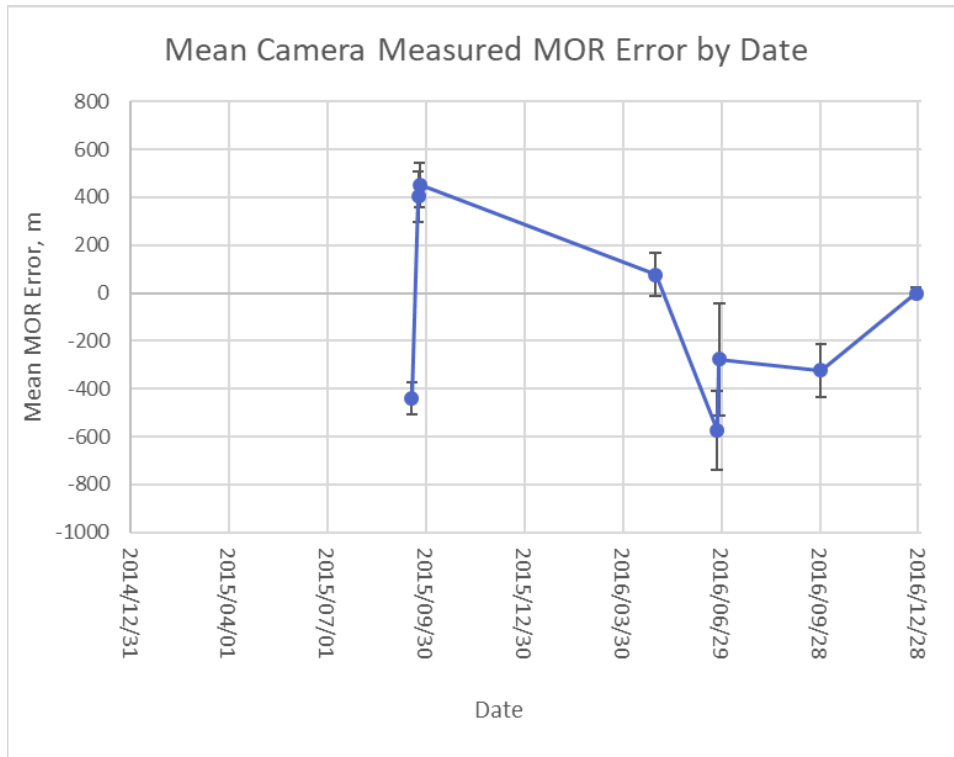
Figure 17. Graph. Changes in the mean camera-measured error by date, and thus season.

DUSK/DAWN ERROR

While it is obvious that the traffic camera would not be able to measure MOR on an unlit roadway like the Smart Road, the performance versus dusk and dawn were unknowns. The data from September 15, 2015, were processed with the calibration from December 26, 2016, and compared with the individual video stills to investigate performance.

Sunrise, and thus dusk and dawn, occur at different times of the day every day and therefore automating the analysis of dusk and dawn was beyond the scope of this effort. On September 15, 2015, the sunrise was around 7:05 a.m. This is an approximate time due to the mountainous terrain in the vicinity of the Smart Road. Civil dawn occurs over the 30 minutes previous to sunrise. Figure 18 illustrates the MOR measured by the camera with respect to the timing of civil dawn. The figure also illustrates another challenge: direct sun impacting the camera. In the case of civil dawn, the camera's automatic settings changed with respect to the increasing lighting, causing a dip in the calculated MOR due to loss of detail. The corresponding video still, Figure 19, shows the lack of detail, particularly compared with the video still from 8 minutes later in Figure 20.
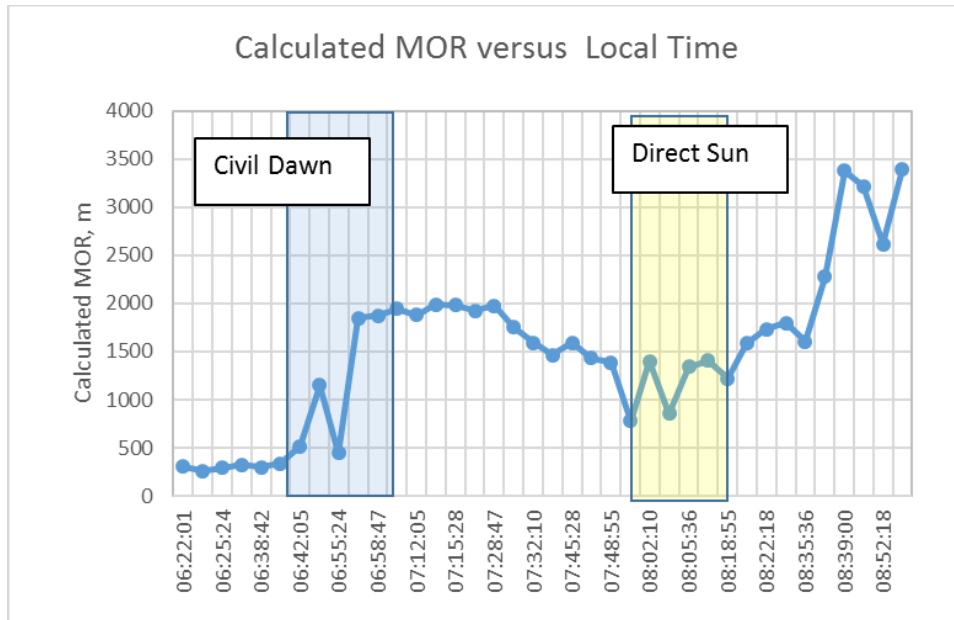
Figure 18**. Graph. Calculated MOR vs. time of day for September 15, 2015, morning detail.**

Figure 19. Photo. Civil dawn camera adjustment, September 15, 2015, 06:55:24 a.m.

Figure 20. Photo. Clear view, September 15, 2015, 7:03:47 a.m.

Figure 18 also shows how direct sunlight causes the camera to adjust to the increased illuminance, reducing the detail on the slope to the left (northeast) of the Smart Road (Figure 21), a typical problem with cameras imaging scenes with large dynamic ranges. In addition, the lens flares and diffraction off dust on the lens of the camera cause bright spots that cover detail in the scene.

Finally, Figure 18 shows another dip in the MOR measurement at 7:37:10 a.m. This corresponds to the scene in Figure 22, where the mountains in the background are washed out. This is due to the large dynamic luminance difference between the sunlit mountains and the foreground, which is still in shadow.

In conclusion, there are considerable MOR measurement errors using a traffic camera with this approach. The calibration approach results in large scatter in the data, particularly for MOR above 500 meters. The Lambertian map does not normalize seasonal scene changes, and there appear to be seasonal variances in the camera measurements, although that could be a function of the large scatter in the data due to the calibration changes.

Figure 21. Photo. Loss of detail due to direct sun, September 15, 2015, 8:03:55 a.m.

Figure 22. Photo. Camera in shade while mountains are sunlit, September 15, 2015, 7:37:10 a.m.

CAMERA PRESET POSITION ERROR

In order to analyze the preset inaccuracy effect on the measurement of MOR, the camera was positioned at a preset position and data were collected for a length of time. Fog events were infrequent and relatively short, taking place near dawn, and the team was unsuccessful at moving the camera during a fog event. Therefore, it was decided that only one move would be used on a sunny day, before the end of the project, to see if there would be an effect on the next fog event. Once it was believed sufficient foggy data had been captured, the camera was moved to the left

(counterclockwise) with pan controls only (no tilt), then commanded to return to the original preset. Data were collected until it was believed a sufficient number of foggy days had occurred for analysis.

In order to minimize the effect of sun position on the lighting of the images, two video stills were selected from nearly the same time on successive days on either side of the camera motion. These are shown on the top and bottom of Figure 23. Both days were sunny with no clouds in the sky.

One image was subtracted from the other and Figure 24 shows a subsequent image representing the difference in the camera images caused by positional inaccuracy and a zoomed-in detail of the difference image. The difference image is black where there is little or no change in the two images, and white where there are large differences in the two images. There are horizontal features all through the image resulting from the lateral shift, a few of which are highlighted by blue rectangles. However, analyzing the near vertical features in the zoomed detail view of the image shows that there is only approximately one pixel change in the image, as highlighted by the red arrows in Figure 24. By summing all of the pixels in the image, it was determined that the difference between the two images was 0.1%. In comparison, the Lambertian map (Figure 5) used to weight the camera view has approximately 10 pixels of vertical smearing. It is therefore unlikely that the effect of the camera preset accuracy will be bigger than the existing error range previously detailed.

Figure 23. Photo. Images used to test camera preset accuracy on camera-based MOR measurement. November 1, 2016, 1:11 p.m. (top), November 2, 2016, 1:13 p.m. (bottom).
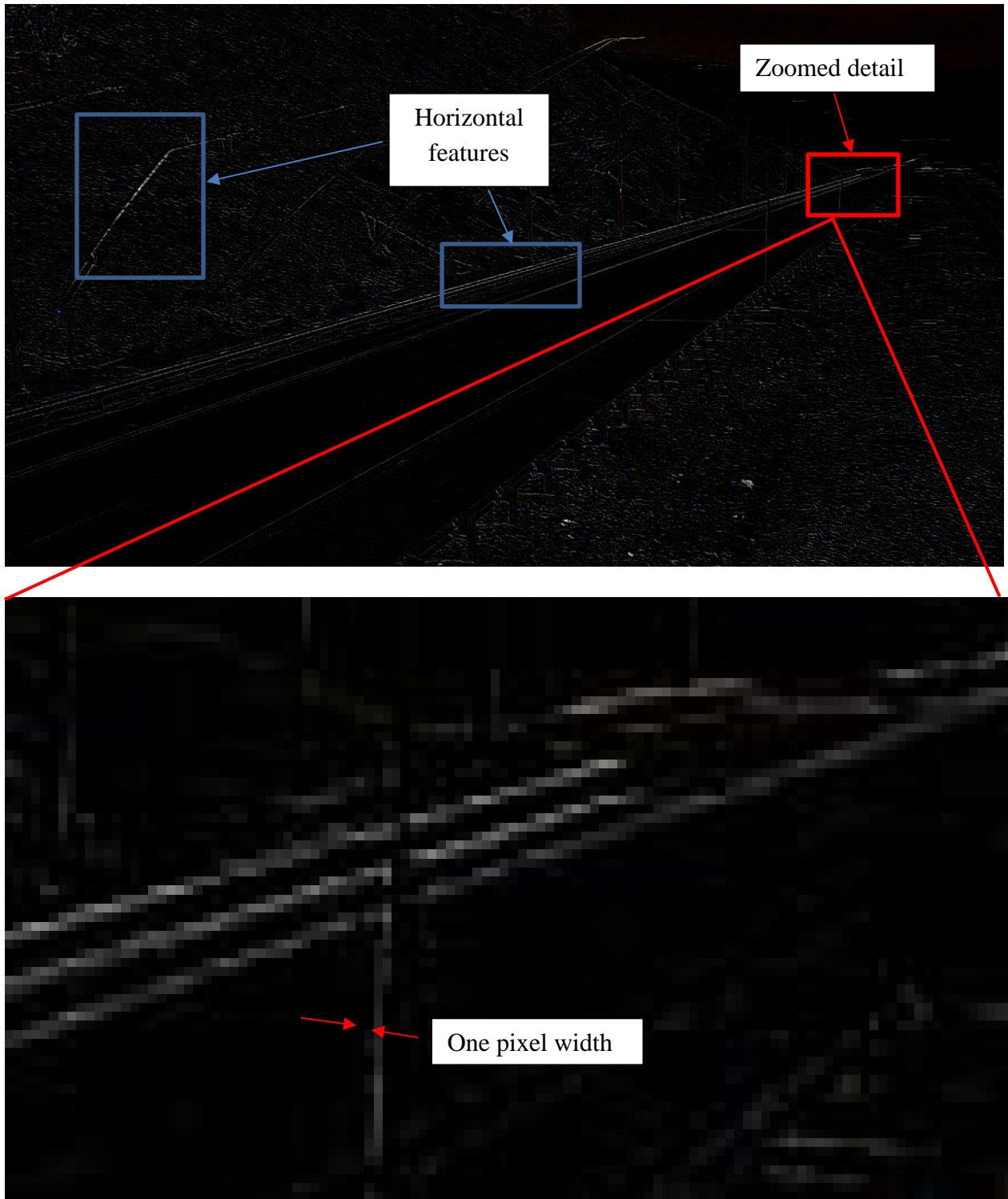
Figure 24. Image. Difference in video stills due to a camera positioning accuracy (top) and detail view (bottom).

After the camera was moved, there was only one foggy day without additional weather: December 26, 2016. Prior to the camera movement, the nearest foggy days with good data were October 6, 2016, and November 29, 2016. The measurements from those three days are shown in Figure 25. Unfortunately, the scatter in the data makes it difficult to determine any differences. Trend lines were fitted in an attempt to interpret the data. As the figure shows, the trend lines from November 29, 2016, and December 26, 2016, which were before and after the camera movement, are similar in slope and offset. However, the scatter in the data from November 29, 2016, is more pronounced. The data for October 6, 2016, seem to correlate well up to MOR equal to 500 meters, but from 500 to 2,000 meters the correlation falls off, resulting in a trend line slope that is different.

Since the data did not show an error, the effect of the change was modeled. For a MOR of 200 meters, the error would be 0.2 meters, and at 2,000 meters the error is approximately 16 meters. These are very small compared to the other errors in the measurements, so it is clear the measurement data will not show the error. In summary, there are differences between the data sets before and after the camera movement. However, a correlation to the error in the camera positions is not possible given the scatter.
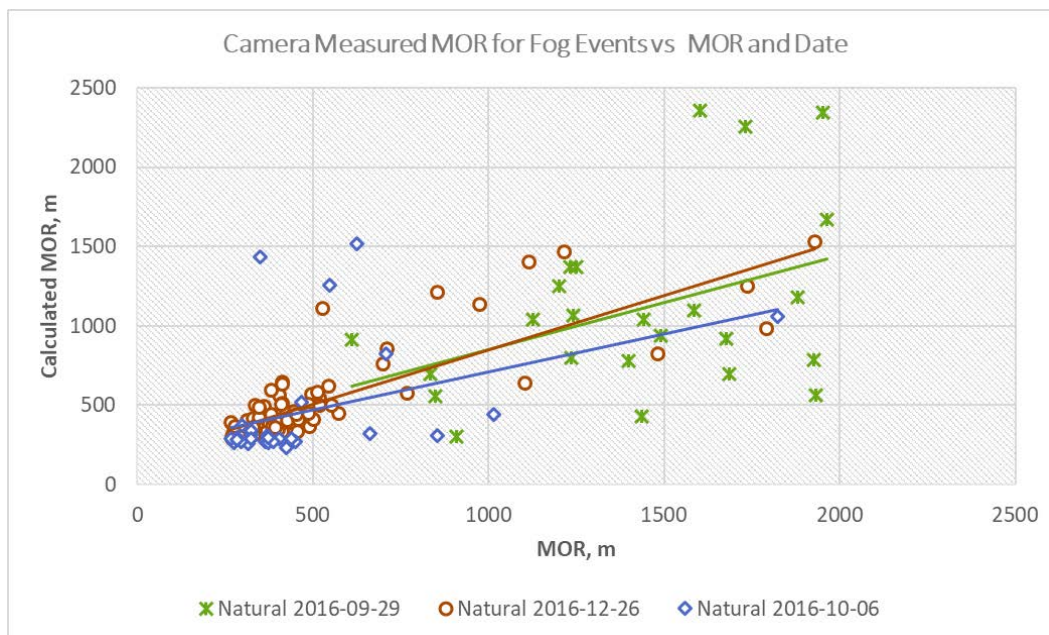
Figure 25. Graph. Comparison of camera-measured MOR before and after camera movement. December 26, 2016, is after; all others are before.

CHAPTER 5. DISCUSSION

This camera-based MOR measurement approach has potential but needs more research for real-world applications. There are calibration challenges as well as large scatter in the measurements at MORs near the upper limit of the calibration capability (2,000 meters). However, there are improvements that could be made in the calibration method, the Lambertian map, and in the machine vision algorithms.

ACCURACY

It is obvious from the data analysis, especially of the 2016 data set, that the one-time calibration of the traffic camera results in errors that render this method of measuring MOR unusable by DOTs. The cyclic pattern to the average errors in the camera-measured MOR suggests that the calibration needs to be generated for each season to account for seasonal changes in the vegetation. One approach to this challenge would be to develop a mobile MOR measurement system that is placed in a location for a short period of time each season to calibrate the cameras four times, one for each season. However, this may not be cost feasible.

Another approach may be to analyze the sunny day data collected from a camera to try to create a model of the changes in the average detail of the scene, use that data to normalize the camera-measured detail, and then apply the calibration. An initial study could be completed using the data set gathered and stored at VTTI.

The scatter in the data above MORs of 500 meters is also a concern. The extremes in the analyzed data were as large as ±1,400 meters of error, indicating that this approach is not ready for implementation as currently designed and deployed. One of the limitations of this approach is that a single-point MOR sensor is used to calibrate a sensor (camera) that makes a volume-averaged measurement of the same quantity. The camera imaged objects between tens of meters away to 1,600 meters away in the same view (the left mountain peak in the images). Variations in the density of the fog over these distances cannot be captured accurately by the calibration instrument, in this study the Vaisala PWD22, because it measures the MOR via light scatter over a physical distance of less than a meter and cannot be located at all locations in view of the camera. No matter where the calibration sensor is placed, it would still be unable to calibrate the entire volume that the camera sees. In addition, the huge variations in the density of the fog in the image stills could be causing the scatter in the measurements of the average detail captured by the camera.

There are two approaches to addressing the calibration sensor limitation. The first is distributing multiple point sensors in the camera's field of view to minimize calibration errors. However, this is not feasible due to the cost. The second approach merits further research. The entire camera view is used to make contrast measurements, which are averaged together in order to reduce error in the contrast measurement. However, the entire view need not be used to make the measurements. The Lambertian map could be reformulated to only include an area in the view that is a manageable distance from the camera and includes diffuse Lambertian objects. For example, the area highlighted in the red rectangle in Figure 26 covers a region approximately 20 meters from the camera at the closest and approximately 100 meters from the camera at the farthest. If the measurement of MOR were limited to only this area, and assuming that the fog

was reasonably uniform across this linear distance, the weather station could be placed at the centroid of the rectangular space for calibration. The space would still include approximately 100 × 400 pixels = 40,000 measurements, and would still be able to reduce the noise in the contrast measurement 200-fold. The result would likely be a much better calibration of the camera-based fog measurement with some impact on <u>potential</u> noise reduction. To work well, the measurement area would need to avoid pavement and vegetation, as they tend to be specular in nature.

Also, the sky area is included in the Lambertian map, but may be a source of error due to partial cloud coverage. Given the challenges with the fog measurement, this was not investigated during this project. However, limiting the measurement area in the camera view will automatically address this concern as well.

Unfortunately, an analysis of the effect of vehicles on the camera-based MOR calculation was not completed during the project due to resource constraints. The camera data include vehicles moving along the test section of the road during clear weather. Since fog is usually avoided as an unnecessary risk during most studies, it is unlikely that camera data included vehicles in natural fog. The 5-minute sample time of the weather station would have made catching a vehicle in the test section when the MOR was known more challenging. That said, the Lambertian map removes most of the roadway from the calculation (Figure 5), and the recommended further reduction in the measurement area will likely prevent vehicles from affecting the MOR measurement. The data captured could be analyzed in the future using some form of machine vision or human-in-the-loop analysis to scan through the 400+ days of video.

Figure 26. Photo. Suggested reduction of camera measurement area.

DUSK/DAWN ERROR

It is not obvious how to overcome the entire challenge of dusk/dawn error without further investigation. During twilight, the camera's performance was less predictable due to automatic gain and shutter changes. This is, however, a relatively short period of time of approximately an hour or less, which may be acceptable given the potential benefits. Should the seasonal uncertainty be solved, this implies that the camera may still only be able to be used between sunrise and sunset. Calibration of the camera's automatic settings may be able to extend the operation range from sunrise to perhaps the start of civil twilight. However, the camera will need artificial lighting to measure MOR during the night. It is not known whether headlights will be sufficient or stable enough for accurate MOR measurement. Another approach may be to use a camera with sensitivity extending into the infrared.

On lighted roadways, the dramatic change in illuminance from day to night will still cause the camera to adjust the settings, causing details to be lost. Unfortunately, this is a hardware limitation. Direct sunlight on a summer day might be 300,000 lux, while highways are lit at night on the order of 30 to 100 lux; it is impossible for traffic cameras to cover this type of range without automatic settings.

Careful calibration of the detail measurement of the camera view in a laboratory setting under changing illumination could address the issue by providing a correction curve based on the gain and shutter settings. However, the same task may be accomplished by further analysis of the camera video data in the VTTI database. The database includes 310 days of data on the performance of the Cohu camera, including many clear-weather dusks and dawns. It is possible that a curve could be developed to correct for the camera settings based on the date and time of day, but this would require additional time and effort.

The camera flares can be addressed by placement of a sun shield or by more careful placement of the camera to avoid directly imaging the sun. Limiting the measurement area, as described above, would also overcome the lens flare issue to some extent and would address the white balance issues cause by the mountain luminance being too high compared to the rest of the scene during the morning hours (Figure 22).

NIGHT USE

Traffic cameras have the potential to measure MOR at night, but this would require data collection on a roadway that is usually lit. Daytime fog is generally more hazardous than nighttime fog due to traffic volume. Roadway lighting would be needed for the approach to work, but was not part of the project scope. Further research is needed to assess the performance of the approach at night with roadway lighting and headlight-only lighting.

CAMERA PRESET ERROR

Camera preset error resulted in approximately one pixel of error vertically. This equated to a 0.1% change in the average detail of the images. The error in MOR from this shift would be less than 0.8% of the measurement. The errors in the measurement of fog MOR on a day the camera was not moved were much larger than the estimated effect of this source of error, resulting in no practical effect of the preset positioning error.

CHAPTER 6. CONCLUSIONS

The approach of using traffic cameras to measure MOR has potential based on the data collected and analyzed during this project. However, the approach investigated, using the entire view of a traffic camera to measure MOR based on a single calibration event was not effective. Due to challenges with the calibration approach, the Lambertian map, and the dusk and dawn transitions, the approach investigated herein was deemed not ready for deployment.

For the data used for calibration, the scatter in the data resulted in errors of hundreds of meters for individual measurements, especially above MORs of 500 meters. Below 500 meters, the error improved, but was still on the order of ±100 to ±200 meters. For other days, the error increased to an extreme of ±1,400 meters. More research work needs to be completed to further optimize the approach before it is ready to consider deployment.

CHAPTER 7. RECOMMENDATIONS

The major recommendation is that the approach of using traffic cameras as a low-cost alternative or additional measurement of inclement weather is not ready for deployment. The data from a single measurement day show potential, but further research is warranted in the following areas in order of priority.

- **Investigation of the reduction of the measurement area, to include a limited measurement volume that reduces the uncertainty due to nonuniformity and calibration errors.** It should be possible to perform this research on the existing data set by limiting the measurement area to the foreground of the camera view nearest to the calibration weather station. This will improve the correlation between the MOR measured by the camera and the MOR measured by the weather station, reduce the scatter, and reduce the impact of the sun.

- **Model the seasonal changes in the scene and Lambertian properties of the scene and develop a cost-effective mitigation or normalization algorithm.** This can be accomplished with the existing data set. The seasonal changes will be most evident in the days with clear weather, so there should be plenty of data to determine the changes. This would work in conjunction with and be enhanced by the first recommendation.

- **Model the dusk and dawn changes in the average measured detail caused by the camera automatic settings and develop a cost-effective interpolation algorithm or normalization scheme based on date and time.** This can be accomplished using the existing data set.

These efforts should dramatically improve the performance of the approach. The data collected by this project illustrate the potential of using traffic cameras to measure MOR, but also highlight the challenges that still need to be addressed for real-world implementation.

APPENDIX A. WEATHER EVENTS CAPTURED IN 2016

Event Date	Event Start	Event End	Event Type	Duration	Intensity	Natural or Simulated	Notes
4/24/2016	6:26 a.m.	9:39 a.m.	Fog	03:13	Light	Natural	High albedo as sun comes up, VERY light fog at station
4/28/2016	7:00 a.m.	7:53 a.m.	Fog	00:53	Light	Natural	No fog at weather station
4/29/2016	6:09 a.m.	8:11 a.m.	Fog	02:02	Heavy	Natural	
4/30/2016	7:18 a.m.	10:48 a.m.	Fog	03:30	Medium	Natural	no video
5/2/2016	5:52 a.m.	8:12 a.m.	Fog	02:20	Medium	Natural	
5/3/2016	6:08 a.m.	8:11 a.m.	Fog	02:03	Light	Natural	No fog at station
5/10/2016	5:51 a.m.	9:38 a.m.	Fog	03:47	Medium	Natural	light fog at station
5/11/2016	5:50 a.m.	7:00 a.m.	Fog	01:10	Medium	Natural	No fog at station
5/11/2016	8:10 a.m.	9:38 a.m.	Fog	01:28	Light	Natural	No fog at station
5/12/2016	5:51 a.m.	9:41 a.m.	Fog	03:50	Light	Natural	
5/14/2016	6:43 a.m.	7:19 a.m.	Fog	00:36	Very Light	Natural	No fog at weather station
5/19/2016	6:08 a.m.	11:41 a.m.	Fog	05:33	Light	Natural	No fog at station
5/20/2016	5:34 a.m.	9:04 a.m.	Fog	03:30	Heavy	Natural	
5/21/2016	5:34 a.m.	8:11 a.m.	Fog	02:37	Medium	Natural	No fog at weather station
5/24/2016	6:27 a.m.	7:54 a.m.	Fog	01:27	Very Light	Natural	light fog at station
5/26/2016	6:43 a.m.	7:18 a.m.	Fog	00:35	Light	Natural	
5/26/2016	8:11 a.m.	8:11 a.m.	Fog	00:00	Light	Natural	No fog at station
5/27/2016	5:33 a.m.	8:11 a.m.	Fog	02:38	Light	Natural	No fog at station
5/28/2016	5:33 a.m.	8:28 a.m.	Fog	02:55	Medium	Natural	
5/30/2016	5:34 a.m.	8:46 a.m.	Fog	03:12	Medium	Natural	
5/31/2016	5:33 a.m.	8:46 a.m.	Fog	03:13	Medium	Natural	
6/19/2016	6:26 a.m.	7:36 a.m.	Fog	01:10	Light	Natural	No fog at weather station
6/23/2016	6:09 a.m.	7:01 a.m.	Fog	00:52	Light	Natural	No fog at weather station
6/24/2016	5:34 a.m.	5:52 a.m.	Fog	00:18	Light	Natural	No fog at weather station

Event Date	Event Start	Event End	Event Type	Duration	Intensity	Natural or Simulated	Notes
6/25/2016	5:15 a.m.	8:28 a.m.	Fog	03:13	Heavy	Natural	
6/26/2016	5:33 a.m.	7:35 a.m.	Fog	02:02	Heavy	Natural	
6/27/2016	5:51 a.m.	8:11 a.m.	Fog	02:20	Medium	Natural	
6/28/2016	6:43 a.m.	7:53 a.m.	Fog	01:10	Light	Natural	No fog at weather station
9/19/2016	7:18 a.m.	8:11 a.m.	Fog	00:53	Light	Natural	No fog at weather station
9/19/2016	8:46 a.m.	9:56 a.m.	Fog	01:10	Light	Natural	No fog at weather station
9/20/2016	6:26 a.m.	9:39 a.m.	Fog	03:13	Heavy	Natural	
9/21/2016	6:43 a.m.	7:36 a.m.	Fog	00:53	Light	Natural	No fog at weather station
9/23/2016	6:44 a.m.	9:22 a.m.	Fog	02:38	Light	Natural	
9/24/2016	7:01 a.m.	7:53 a.m.	Fog	00:52	Light	Natural	No fog at weather station
9/28/2016	7:01 a.m.	8:29 a.m.	Fog	01:28	Medium	Natural	No fog at weather station
9/29/2016	6:43 a.m.	9:05 a.m.	Fog	02:22	Light	Natural	
9/29/2016	6:59 p.m.	7:34 p.m.	Fog	00:35	Heavy	Natural	
10/1/2016	6:43 a.m.	8:39 a.m.	Fog	01:56	Medium	Natural	
10/2/2016	7:21 a.m.	8:21 a.m.	Fog	01:00	Very Light	Natural	No fog at weather station
10/3/2016	6:38 a.m.	9:20 a.m.	Fog	02:42	Very Light	Natural	
10/4/2016	7:00 a.m.	8:06 a.m.	Fog	01:06	Very Light	Natural	No fog at weather station
10/6/2016	6:44 a.m.	10:14 a.m.	Fog	03:30	Heavy	Natural	
10/11/2016	6:26 a.m.	8:28 a.m.	Fog	02:02	Light	Natural	No fog at weather station
10/12/2016	7:53 a.m.	9:03 a.m.	Fog	01:10	Medium	Natural	No fog at weather station
10/14/2016	7:02 a.m.	8:47 a.m.	Fog	01:45	Medium	Natural	No fog at weather station
10/14/2016	9:04 a.m.	10:15 a.m.	Fog	01:11	Light	Natural	No fog at weather station
10/16/2016	7:01 a.m.	9:39 a.m.	Fog	02:38	Light	Natural	No fog at weather station
10/18/2016	7:00 a.m.	9:55 a.m.	Fog	02:55	Medium	Natural	No fog at weather station
10/19/2016	8:12 a.m.	9:39 a.m.	Fog	01:27	Light	Natural	No fog at weather station
10/20/2016	7:01 a.m.	10:11 a.m.	Fog	03:10	Light	Natural	No fog at weather station
10/29/2016	8:29 a.m.	9:55 a.m.	Fog	01:26	Light	Natural	No fog at weather station

Event Date	Event Start	Event End	Event Type	Duration	Intensity	Natural or Simulated	Notes
11/2/2016	7:18 a.m.	11:58 a.m.	Fog	04:40	Light	Natural	Moved Camera 40 degrees to the left and then back to Preset 1 at 11:13:20
11/5/2016	8:10 a.m.	9:38 a.m.	Fog	01:28	Light	Natural	No fog at weather station
11/7/2016	7:18 a.m.	9:21 a.m.	Fog	02:03	Light	Natural	No fog at weather station
11/17/2016	7:01 a.m.	9:04 a.m.	Fog	02:03	Light	Natural	No fog at weather station
11/18/2016	7:36 a.m.	8:46 a.m.	Fog	01:10	Light	Natural	No fog at weather station
11/19/2016	7:18 a.m.	9:56 a.m.	Fog	02:38	Light	Natural	No fog at weather station
11/25/2016	8:10 a.m.	10:13 a.m.	Fog	02:03	Light	Natural	No fog at weather station
11/30/2016	7:02 a.m.	9:39 a.m.	Fog	02:37	Medium	Natural	Before daybreak
12/25/2016	7:02 a.m.	8:29 a.m.	Fog	01:27	Light	Natural	
12/26/2016	7:17 a.m.	2:53 p.m.	Fog	07:36	Medium	Natural	
12/26/2016	5:13 p.m.	5:20 p.m.	Fog	00:07	Light	Natural	
12/28/2016	7:01 a.m.	7:19 a.m.	Fog	00:18	Light	Natural	

REFERENCES

1. Babari, R., N. Hautière, É. Dumont, N. Paparoditis, and J. Misener. Visibility monitoring using conventional roadside cameras–Emerging applications. *Transportation Research Part C: Emerging technologies*, Vol. 22, 2012, pp.17-28.

2. American Association of State Highway and Transportation Officials (AASHTO). *Green Book: A Policy on Geometric Design of Highways and Streets*, 5th ed. AASHTO, Washington, D. C., 2004.